Multiscale selectivity and in vivo biodistribution of NRP-1-targeted theranostic AGuIX nanoparticles for PDT of glioblastoma

Mickaël Gries, Noémie Thomas, Joël Daouk, Paul Rocchi, Laurence Choulier, Justine Jubréaux, Julien Pierson, Aurélie Reinhard, Valérie Jouan-Hureaux, Alicia Chateau, et al.

To cite this version:

Mickaël Gries, Noémie Thomas, Joël Daouk, Paul Rocchi, Laurence Choulier, et al.. Multiscale selectivity and in vivo biodistribution of NRP-1-targeted theranostic AGuIX nanoparticles for PDT of glioblastoma. International Journal of Nanomedicine, 2020, 15, pp.8739-8758. 10.2147/IJN.S261352 . hal-02995133

HAL Id: hal-02995133
https://hal.science/hal-02995133v1

Submitted on 26 Nov 2020

International Journal of Nanomedicine

Dovepress
open access to scientific and medical research

Open Access Full Text Article

ORIGINAL RESEARCH

Multiscale Selectivity and in vivo Biodistribution of NRP-1-Targeted Theranostic AGuIX Nanoparticles for PDT of Glioblastoma

This article was published in the following Dove Press journal:
International Journal of Nanomedicine

Mickaël Gries[1]
Noémie Thomas[1]
Joël Daouk[1]
Paul Rocchi[2]
Laurence Choulier[3]
Justine Jubréaux[1]
Julien Pierson[1]
Aurélie Reinhard[1]
Valérie Jouan-Hureaux[1]
Alicia Chateau[1]
Samir Acherar[4]
Céline Frochot[5]
François Lux[2–6]
Olivier Tillement[2]
Muriel Barberi-Heyob[1]

[1]Université de Lorraine, Centre National de la Recherche Scientifique (CNRS), Research Center for Automatic Control of Nancy (CRAN), Nancy, France; [2]Université de Lyon, CNRS, Institut Lumière Matière, Lyon, France; [3]Université de Strasbourg, CNRS, Biotechnologie et Signalisation Cellulaire, Illkirch, France; [4]Université de Lorraine, CNRS, Laboratoire de Chimie-Physique Macromoléculaire, Nancy, France; [5]Université de Lorraine, CNRS, Laboratoire Réactions et Génie des Procédés, Nancy, France; [6]Institut Universitaire de France, Paris, France

Background: Local recurrences of glioblastoma (GBM) after heavy standard treatments remain frequent and lead to a poor prognostic. Major challenges are the infiltrative part of the tumor tissue which is the ultimate cause of recurrence. The therapeutic arsenal faces the difficulty of eradicating this infiltrating part of the tumor tissue while increasing the targeting of tumor and endogenous stromal cells such as angiogenic endothelial cells. In this aim, neuropilin-1 (NRP-1), a transmembrane receptor mainly overexpressed by endothelial cells of the tumor vascular system and associated with malignancy, proliferation and migration of GBM, highlighted to be a relevant molecular target to promote the anti-vascular effect of photodynamic therapy (VTP).

Methods: The multiscale selectivity was investigated for KDKPPR peptide moiety targeting NRP-1 and a porphyrin molecule as photosensitizer (PS), both grafted onto original AGuIX design nanoparticle. AGuIX nanoparticle, currently in Phase II clinical trials for the treatment of brain metastases with radiotherapy, allows to achieve a real-time magnetic resonance imaging (MRI) and an accumulation in the tumor area by EPR (enhanced permeability and retention) effect. Using surface-plasmon resonance (SPR), we evaluated the affinities of KDKPPR and scramble free peptides, and also peptides-conjugated AGuIX nanoparticles to recombinant rat and human NRP-1 proteins. For in vivo selectivity, we used a cranial window model and parametric maps obtained from T2*-weighted perfusion MRI analysis.

Results: The photophysical characteristics of the PS and KDKPPR molecular affinity for recombinant human NRP-1 proteins were maintained after the functionalization of AGuIX nanoparticle with a dissociation constant of 4.7 µM determined by SPR assays. Cranial window model and parametric maps, both revealed a prolonged retention in the vascular system of human xenotransplanted GBM. Thanks to the fluorescence of porphyrin by non-invasive imaging and the concentration of gadolinium evaluated after extraction of organs, we checked the absence of nanoparticle in the brains of tumor-free animals and highlighted elimination by renal excretion and hepatic metabolism.

Conclusion: Post-VTP follow-ups demonstrated promising tumor responses with a prolonged delay in tumor growth accompanied by a decrease in tumor metabolism.

Keywords: vascular photodynamic therapy, AGuIX nanoparticle, NRP-1, peptide, brain tumors, glioblastoma, radiation therapies

Introduction

GBM is the most common and aggressive primary brain tumor in adults, characterized by an extremely poor prognosis.[1] According to Stupp et al,[2] newly diagnosed GBM patients with a favorable Karnofsky performance scale receive standard

Correspondence: Muriel Barberi-Heyob
Email muriel.barberi@univ-lorraine.fr

submit your manuscript | www.dovepress.com
DovePress
http://doi.org/10.2147/IJN.S261352

treatment consisting of maximal surgical resection followed by postoperative radiation with concomitant and adjuvant temozolomide therapy. Diagnosis is established by magnetic resonance imaging (MRI), playing also a central role to define and delineate the target volume for radiotherapy, but producing typically irregular contrast enhancement.[3] Despite advances in the diagnosis and treatment, recurrence is almost inevitable, and the prognosis remains poor, less than fifteen months.[4] It remains particularly difficult to treat because of the intrusive penetration of isolated cells into adjoining tissues.[5] This invasive infiltrative disease component is the ultimate cause of recurrence, resistance and death. At the time of recurrence, no standard of care or therapeutic consensus exists. Treatment options stand limited with modest benefits, consisting of repeating first line treatment options (surgery or/and radiotherapy) or new therapeutic arsenal as systemic therapy or combination therapy. However, since radiotherapy is a therapy with a narrow therapeutic window, many limitations must be considered. External photon radiotherapy being non-specific, a significant dose can be too important to the surrounding healthy brain tissue, increasing the risk of necrosis of the normal brain tissue.

With the rapid development of nanomedicine for cancer applications, it is expected that newly developed metal-based nanoparticles could have a major impact on GBM therapy and imaging-guided treatment through selective destruction of neoplastic cells while minimizing damage to healthy tissue.[6] Exploiting the EPR effect, a new generation of inorganic nanoparticles containing magnetic properties appears as very promising systems, offering new opportunities to overcome the limitations of current GBM management options in clinic. In the context of brain tumors, gadolinium (Gd)-based nano-objects suggest promising prospects in clinical practice as AGuIX technology.[7,8] AGuIX nanoparticles consist of a polysiloxane matrix with DOTAGA-Gd^{3+} chelates on their surface for a hydrodynamic diameter close to 5 nm, allowing a rapid renal clearance.[7] Their paramagnetic properties usable in MRI gives them the possibility of evaluating the intra-tumoral distribution of nanoparticles.[9] Passive targeting of original AGuIX nanoparticles for tumor tissue is well known and was rigorously studied on rodents and safety on non-human primate models was shown before going to the clinical trial (phase II with whole brain radiation therapy (WBRT) in multiple metastasis; NCT04094077;[8] and phase II to evaluate their clinical impact in combination with fractionated stereotactic radiation in oligo brain metastases).[10] Due to their small size, AGuIX nanoparticles can indeed quickly accumulate and be retained in the tumor by EPR effect.[11] However, the quantity of nanoparticles reaching the tumor area and their residence time into the tumor tissue remain variable and widely influenced by its vascularization. Since its discovery in 1981 by Maeda et al,[12] EPR effect has long been considered as a safe, simple and effective means for the delivery of anticancer nanomedicine. Despite very promising potential in the preclinical phases, recent clinical trials outcomes have remained heterogeneous. The inter- and intra-individual heterogeneity in EPR-mediated tumor targeting, leading to a low concentration of nanoparticles in the tumor tissue and the disparity between in vivo models and clinical reality, remain the main obstacles which limit this passive targeting strategy.[13,14] Consequently, the heterogeneity of the accumulation of AGuIX nanoparticles due to the unpredictability of the EPR effect and sometimes their low tumor residence times, tend to consider active targeting, especially in the strategic infiltrative areas of GBM tumors.[15] Active targeting strategies using, for instance, specific ligands such as antibodies or peptides could be a solution to overcome these limitations.

For endothelial cells expressing an angiogenic phenotype, transmembrane receptors such as receptors to VEGF-A (vascular endothelial growth factor-A), can be suggested as molecular targets for GBM. Our group recently designed AGuIX nanoparticles covalently grafted with a ligand peptide motif (KDKPPR) targeting the VEGF receptor NRP-1. This transmembrane receptor has received significant attention as a potential therapeutic target in GBM.[16] Increased NRP-1 expression in GBM biopsies correlates with increased malignancy, whereas reducing its expression suppresses migration, proliferation and survival in vitro, cancer stem cells (CSC) viability and tumor growth in vivo.[17] Moreover, NRP-1 has also been shown to function as a co-receptor for VEGF-R on glioma-associated macrophages (GAM) where it plays a key role in the accumulation of immunosuppressive and pro-angiogenic macrophages at sites of tumor hypoxia.[18]

In the context of GBM and compared to standard therapeutic strategies, photodynamic therapy (PDT) appears to be an alternative or complementary approach that may reduce recurrence and improve the overall survival of patients.[19–23] Using an appropriate wavelength, the photodynamic process consists on the excitation of PS molecules in order to generate in situ the production of reactive oxygen species (ROS), in particular singlet oxygen, the most important cytotoxic agent generated during PDT. The chemical nature of the photoactivatable compound is essential to induce an effectiveness of the treatment as most of them are water insoluble and have a low in vivo selectivity for the tumor tissues. Conversely, certain nanoparticles can accumulate specifically in the tumor tissue thanks to the EPR effect, and moreover, they can be functionalized for active targeting. Moreover, their chemical composition can be adapted to protect PS molecules, increase their solubility in biological media and optimize their pharmacokinetic properties.[24] By adding in the same nano-object, a contrast agent such as gadolinium to PS molecules, an image-guided PDT can be performed to construct the tumor volume, plan the treatment, optimize the drug-light interval before light exposure and assess the tumor response by longitudinal diffusion MRI.[25]

Numerous studies also showed the major role of the vascular effect in tumor eradication by a photodynamic process. This strategy called VTP allows a local control.[25,26]

In this article, we highlighted the molecular, cell and tissue selectivity of multifunctional AGuIX-like nanoparticle (AGuIX@PS@KDKPPR). This nanoparticle consists of an AGuIX design skeleton onto which has been grafted porphyrin molecules as PS agent and KDKPPR as targeting peptide.[27,28] This peptide moiety has been previously optimized by our group from a screening methodology based on the sequence homology of the domain encoded by exon 8a of $VEGF_{165}$.[29] As affinity for NRP-1 receptor is an essential condition for VTP, emphasis has been placed on specific reference methods, namely SPR and complementary in vivo techniques such as a cranial window chamber model in order to face the obstacles inherent in brain tumors (blood-brain/tumor barrier). We also assessed the impact of the peptide grafting on biodistribution, elimination processes and on nanoparticle accumulation into the tumor area. Facilitated by the nature of AGuIX@PS@KDKPPR nanoparticle, MR and fluorescence imaging have been combined for this purpose. The interest of the approach, in terms of efficiency, was the last point to study.

Materials and Methods

Nanoparticles Synthesis and Characterization

All reactions involving porphyrin compounds were carried out away from light. Nanoparticles synthesis and their characterization have been previously described in Thomas et al[27] and Toussaint et al.[25] Briefly, synthesis consisted in the coupling of a maleimido-PS@KDKPPR with AGuIX-SH. The size distribution and zeta potential of the nanoparticles were performed by Dynamic Light Scattering (DLS) using the Zetasizer NanoS DLS (laser He-Ne 633 nm) from Malvern Instrument. Relaxation time was measured using a Bruker Minispec MQ60 NMR analyzer (Bruker, Ettlingen, Germany), operating at 1.4 T magnetic field. For their photophysical properties, all the compounds were diluted in a solution of deuterium oxide (D_2O) (Merck, Darmstadt, Germany). The absorption spectra were carried out with a UV-visible Perkin-Elmer spectrophotometer (Lambda 2, Courtaboeuf, France) and the fluorescence spectra by a Fluorolog-3® spectrofluorimeter (Jobin Yvon, Longjumeau, France) equipped with a 450-Watt Xenon lamp. Hydrophilic and hydrophobic characteristics were also evaluated using the "shake flask". Fluorescence and singlet oxygen quantum yields were calculated as previously described in Kamarulzaman et al.[30]

For in vivo studies, nanoparticles were suspended in ultrapure water at concentration of 8 mM porphyrin equivalent and 110 mM Gd equivalent. Injected porphyrin amounted to 1.75 $\mu mol.kg^{-1}$ (for PDT) (ie, 35 $\mu mol.kg^{-1}$ Gd equivalent) or 4 $\mu mol.kg^{-1}$ (ie, 80 $\mu mol.kg^{-1}$ Gd equivalent) (for distribution and selectivity experiments) in 9% sodium chloride (NaCl) as previously described in Toussaint et al.[25] All nanoparticle preparations were injected by intravenous administration in the caudal vein.

U87 Cell Culture and Transfection

The human GBM U87 cell line (ATCC® HTB-14™) was purchased from the American Type Culture Collection (Molsheim, France). Cells were grown in Dulbecco's modified Eagle's medium low glucose (Gibco, France), penicillin (100 $U.mL^{-1}$) (Gibco, France), streptomycin (100 $g.mL^{-1}$) (Gibco, France), supplemented with 10% fetal bovine serum (Sigma-Aldrich, France) and 5% of a commercial supplement, containing non-essential and essential amino acids, vitamins and sodium pyruvate (Sigma-Aldrich, France). Cells were maintained in a 5% CO_2 humidified incubator at 37°C. For transfection, U87 cells were seeded at 50,000 cells.cm-2 and cultured for two days without changing the media. At 90% confluence, the cells were treated with 10 µL of recombinant adenovirus Ad CMV eGFP (Kerafast, Inc., Boston, MA) for 24h. The validation of adenovirus infection was then carried out by visualization with a fluorescent microscope (Nikon microscope AZ100 system equipped with a Digital Light DS-Qi1Mc camera and a confocal device).

3D U87-GFP Spheroid Model

U87-GFP cells were seeded at 1000 cells/cm2 in four T75 flask previously coated with polyhydroxyethylmethacrylate (polyHEMA) at a concentration of 20 mg.mL^{-1} to prevent the cells from adhering to the support. After 3 days, the cell suspensions were transferred to a 500 mL spinner (Magnaflex, Wheaton Science) placed on a magnetic stirrer (MultiMagStir Genie, Model SI-300, Scientific Industries) set to 70 rpm with constant stirring. The suspension was passed through a nylon filter whose pores measure 100 µm after four days to keep only the spheres larger than 100 µm. Finally, six days later, the spheroids were collected then filtered successively by two filters of different porosity: one of 380 µm and one of 520 µm. Only the spheroids being between these two sizes were kept for their implantation in the nude mice brain.

SPR Experiments

All experiments were performed on a Biacore T200 instrument (GE Healthcare Biacore, Uppsala, Sweden) at 25°C. Sensor surfaces and other Biacore consumables were purchased from GE Healthcare Biacore (USA). IgG1, and recombinant human/rat NRP-1 proteins were purchased from R&D Systems (Inc., Minneapolis, USA). The detection of binding and the measurement of kinetic parameters between nanoparticles and NRP-1 protein were examined by the Biacore T200 System. CM5 Sensor Chip was activated by using sulfo-NHS/EDC (1-ethyl-3-[3-dimethylaminopropyl] carbodiimide) solution (0.2 µM) in PBS (phosphate-buffered saline) with 0.05% ($^{v}/_{v}$) surfactant P20, pH 7.4. The chip was subsequently immobilized with the recombinant human NRP-1 protein (MW: 70900 Da) or IgG1 (as control, MW: 26600 Da) at a concentration of 50 µg.mL^{-1} in sodium acetate (pH 4.0) or with the recombinant rat NRP-1 (MW: 11900 Da) protein at a concentration of 50 µg.mL^{-1} in formate (pH 3.0) at flow rate of 5 µL/min for 10 min. Immobilization levels were 4020 resonance units (RU) for IgG1, 9556 RU for rat NRP-1 and 10124 RU for human NRP-1 proteins. The chip was then blocked with 1 M of ethanolamine, pH 8.0. Analytes previously dissolved in ultrapure water at 4 mM were diluted in running buffer at concentrations ranging from 0.625 µM to 80 µM. The compounds were flowed at a rate of 30 µL.min^{-1} for 300 s to allow association, followed by 300 s of dissociation at 25°C. Each compound injection was followed by a 120 s buffer flow and a 5 s, 5 mM HCl injection for surface regeneration. Sensorgrams were corrected for signals from the control (simple referencing). The equilibrium response was recorded 5 s before the end of the compound injection (time window: 5 s). The K_D value was determined by fitting the response versus analyte concentration curve to a simple 1:1 interaction model with the Biacore T100 2.0.2 evaluation software (GE Healthcare). Results were presented as mean of two independent experiments.

Animal Care and Ethics Statement

All in vivo experiments were realized in accordance with the European Community animal care guidelines (Directive 2010/63/EU) for the use of experimental animals with respect to the 3 Rs' requirements for Animal Welfare and carried out by competent and authorized persons in a registered establishment (establishment numbers D-54-547-03 issued by the Departments of Veterinary Services). All protocols and procedures involving the use of animals were examined and validated by an internal ethics committee (Comité d'Ethique Lorrain en Matière d'Expérimentation Animale, CELMEA, French Ethical Committee number 66) in accordance with national regulations (the research project APAFIS #15535 and APAFIS #20985 were approved by the French Ministry of Research). Animals were kept under standard conditions (T =24°C±1°C, hygrometry 50%±10%, controlled 12h light–dark cycle) and had free access to standard. Six weeks old nude male rats (Hsd: RH-Foxn1rnu) and six weeks old NMRI nude female mice were purchased from Envigo (Netherlands) and Janvier Labs (France), respectively.

Orthotopic Model

Stereotactic U87 xenograft implantation was previously described by Toussaint et al.[25] Briefly after a midline incision, a burr hole was drilled and a skull anchor (Patent N° 11 55596) was fixed. 5.10^{4} U87 cells were injected into the brain parenchyma, the scalp incision was sutured, and the surface was antiseptically cleaned. A total of 42 rats were xenografted in order to perform the different approaches such as MRI analysis, MRI-guided interstitial PDT and ^{18}F-FDG-PET (positron emission tomography) acquisitions.

Cranial Chamber Model with U87-GFP Spheroid and Fluorescence Imaging

After mice anesthesia, skin above the skull was incised, the periosteum gently removed, and a 4 mm diameter circle was drilled in the interest area in the skull (located between bregmatic, sagittal and lambdoid sutures). After removing the bone flap, a U87-GFP spheroid was placed in a breach in the cerebral parenchyma. Brain and skull were kept humidified via physiological saline solution throughout the procedure. A glass slice (5 mm diameter) was then placed to cover the brain and was stuck to the skull with surgical cyanoacrylate glue. Finally, a thin layer of dental acrylic was applied over the entire surface of the skull and a small edge of the coverslip. After 10–14 days following U87-GFP spheroid implantation, mice were divided into two batches: AGuIX@PS@KDKPPR or AGuIX@PS@scramble group. Visualization of the localization of different nanoparticles into the vasculature (lumen versus vascular column) was performed on anesthetized mice before and at 1, 4 and 24 h after injection using the Nikon microscope AZ100 (Nikon Corp., Tokyo, Japan) system equipped with a Digital Light DS-Qi1Mc camera and a confocal device (Revolution DSD; Andor Technology, Belfast, UK).

The excitation filter was at 560 ± 25 nm for the free PS or conjugated on nanoparticles and at 475 ± 20 nm for the GFP-U87 fluorescent images acquisition. The emission filter was composed with a block of four emission filters at 440, 521, 607 and 700 nm.

MRI Analysis

At about 10–14 days after stereotactic U87 xenograft implantation rats bearing tumor were imaged using a small animal 7 Tesla magnet (BioSpec 70/20 USR; Bruker Optik GmbH, Ettlingen, Germany). The software Paravision 5.2 (Bruker, Ettlingen, Germany) was used to analyze the data. All Rats were maintained anesthetized throughout the procedure.

T2-weighted imaging (TURBO-Rapid Acquisition with Relaxation Enhancement (repetition time) TR/(echo time) TE: 5000/77 ms, NEX: 2, FOV: 4x4 cm, slice thickness: 1 mm, matrix: 256x256) in axial, coronal and sagittal planes were performed to locate the tumor appearing in hypersignal, to measure the coordinates for the fiber placement for interstitial PDT and to monitor the tumor response to the treatment from pre-treatment until the day the tumor has reached more than 2 times the initial volume.T1-weighted imaging (RARE acquisition; relaxation enhancement TR/TE =400/9-10 ms; slice thickness: 1.5 mm; matrix: 256×256) repeated before and after intravenous injection of nanoparticles (AGuIX@PS@KDKPPR, AGuIX@PS@scramble or AGuIX injection at 80 µmol·kg^{-1}, gadolinium equivalent) in axial planes to visualize the tumor tissue in hyperintense and in coronal planes highlighted the presence of the gadolinium in the kidney and the bladder. The abdominal acquisitions were realized with fat saturation and respiratory gating. 3D coronal flash acquisition (relaxation enhancement TR/TE = 200/3 ms; slice thickness: 0.2 mm, matrix: 256×256) were performed for dynamic perfusion study. The resulting gadolinium-enhanced perfusion series consisted of 45 images per slice including 5 images before nanoparticles injection (AGuIX, AGuIX@PS@KDKPPR or AGuIX@PS@scramble) and 40 images after injection. MRI data were transferred in DICOM format and analyzed under ImageJ. MR signal is made up of the combined T1- and T2- effects of gadolinium-based contrast agent. So, the measured relaxivity change ΔR2* can be defined by:

$$\Delta R_2^* = \left(\frac{-1}{TE}\right) \times \mathrm{Ln}\left[\frac{S(t)}{S_0}\right]$$

where TE is echo time, S(t) the signal in the tumor over the time and S_0 the baseline of S(t) before the passage of the bolus.[31] The implemented algorithm is based upon a pixel-by-pixel scheme. The first step of the computation consisted in the creation of the mask of the cerebellum (as control) and the mask of the tumor by manual thresholding. For each pixel, the pre-bolus baseline S_0 was estimated by averaging 5 time-points before bolus. Then, the relaxivity time curve was computed for all the pixels within the mask. In addition to this, mean transit time (MTT) has been calculated as the first moment of the relaxivity time curve.

Distribution and Elimination by Fluorescence Intensity Analysis

The experiments were performed by platform named Optimal (Grenoble, France) specialized in optical imaging of small animals. After 24h or 96h post-intravenous (i.v.) injection of AGuIX@PS@KDKPPR, mice were euthanized and several organs (brain, heart, lung, spleen, uterus-ovaries, skin, muscle, abdominal fat, kidney, bladder and liver), plasma and ganglia (right and left brachial ganglia, right and left axillary ganglion, mesenteric ganglion and right and left inguinal ganglion) were collected. Fluorescence imaging was performed with a 2D-fluorescence imaging device (IVIS Kinetic, PerkinElmer, USA) with excitation and emission wavelengths at 430 and 720 nm, respectively. Semiquantitative data were obtained using the Wasabi® software (Hamamatsu, Massy, France) by drawing regions of interest (ROIs) on the different organs and were expressed as the number of Relative Light Units (R.L.U.) per pixel per unit of exposure time and relative to the fluorescence signal in the skin. Three mice have been necessary for each time. Control mice were sacrificed to quantify organs autofluorescence.

Ex vivo Gadolinium Quantification by ICP-MS

The ICP-MS (Inductively Coupled Plasma Mass Spectrometry) assay was performed by the Eurofins Expertise Environmental Laboratory in Maxéville. After 24h or 72h post- i.v. injection of AGuIX@PS@KDKPPR, mice were euthanized and their organs (brain, skin, kidney and liver) and whole blood were collected. The sample underwent wet digestion with 10 mL of nitric acid (HNO_3) for 1h, and then, mineralization consisting of heater at 104°C for 120 min. In each sample, Gd concentration was measured by ICP-MS system ELAN® DRC II (PerkinElmer Inc., Waltham, MA). Verification of the ICP-MS system was performed using a linear regression graph of different concentrations of a standard Gd solution. The limit of quantification of Gd concentration was determined at 5 $\mu g.L^{-1}$ based on pulse intensity of Gd standard solution. Organ-specific Gd concentration values were calculated as percent injected dose per gram of tissue (% $ID.g^{-1}$) as:

$$\%\frac{ID}{g} = \frac{\left(\frac{Gd_{organ}}{Gd_{injected}}\right)}{M_{organ}}$$

where Gd_{organ} was the mass of Gd found in the organ, $Gd_{injected}$ the mass of Gd injected and M_{organ} the mass of the organ. Three mice have been necessary for each group (24h or 72h after i.v. injection). Results were presented as mean and standard deviation.

MRI-Guided Interstitial PDT

When the tumor reached approximately 6 ± 1 mm of diameter, PDT could be delivered under MRI guidance. To deliver illumination, a silica optical fiber, UltraSil 272 ULS (OFS, Norcross, GA), which had a diameter of 272 nm and a numerical aperture of 0.29, was inserted into the brain through the cannula of the anchor at the predetermined depth (at the top of the tumor). Before illumination, the optical fiber position was confirmed by a coronal and sagittal proton density-weighted MRI acquisition. The drug-light interval (DLI) and laser light settings were chosen to be optimal according to the nanoparticles. With a rapid elimination out of the tumor and based on an experimental design work,[27] the AGuIX-PS were excited 1h after intravenous injection with light emitted at 652 nm (50 mw, 8 min 40 s, 26 J). For AGuIX@PS@KDKPPR, the drug-light interval was postponed to 4h in order to avoid activation of free porphyrin in the circulation with light emitted at 652 nm (fluence rate 40 mW, fluence 20.8 J). Different control groups were followed to distinguish the potential effects on tumor growth; (i) rats exposed to light after injection of AGuIX nanoparticles (n=3), (ii) rats injected only with AGuIX@PS@KDKPPR nanoparticles without light exposure (n=5) and, (iii) rats without any treatment (n=6). These groups were pooled together as control group (n=14) due to the absence of impact on tumor growth. The two other groups were rats receiving interstitial PDT with AGuIX@PS (n=9) or with AGuIX@PS@KDKPPR (n=7).

^{18}F-FDG-PET Acquisition

Positron emission tomography (PET) recordings were obtained with a camera dedicated to small animal studies (Inveon, Siemens Preclinical Solutions, Knoxville, USA). After rat anesthesia, 65 MBq of ^{18}F-FDG were injected as a bolus via a lateral tail vein cannulation. List-mode acquisitions of 120 min durations were initiated a few seconds prior to tracer injection, and the acquired PET data were subsequently reconstructed in 27 consecutive frames (ie, 5 frames of 120-s duration followed by 22 frames of 5-min duration) using the ordered-subsets expectation maximization 3D algorithm (OSEM3D, 4 iterations, 16 subsets, zoom 1) together with scatter and attenuation corrections based on transmission source measurement. The final voxel size was $0.8 \times 0.8 \times 0.9$ mm^3. In addition, the 27 frames were averaged for manual registration with T2 coronal images. Tumors were segmented on MRI images and contours were plotted on average PET images. Tumor and healthy brain tissue activities were determined through mean standardized uptake values (SUV) within volume of interests (VOI), which were drawn with a dedicated software (Inveon Research Workplace 4.1, Siemens®, Knoxville, USA) on the fusion images encompassing the entire 120-min recording period and MRI acquisitions previously performed. VOIs were placed inside the tumor and contralateral healthy brain tissue regions with the VOI limits approximating the organ limits as close as possible.

Statistical Analysis

Efficacy of PDT was presented with the Kaplan-Meier model, considering the percentage of tumors not having reached 2 times their initial volume as the endpoint. Statistical analysis was conducted through the Log rank test using GraphPad Prism 5 (GraphPad Software, USA). All results were given as mean ± standard error of the mean (SEM).

Results and Discussion

Physicochemical Characterization and Photophysical Properties

A mean hydrodynamic diameter at about 11.1 nm was measured for the three functionalized nanoparticles illustrated in Figure 1A and named AGuIX@PS, AGuIX@PS@KDKPPR and AGuIX@PS@scramble. The grafting of the porphyrin molecule alone or combined with the peptide moiety induced a hydrodynamic diameter twice as large as the original AGuIX particle, ie, 4.9 nm on average. Moreover, as presented in Table 1, the resulting nanoparticles have a mean hydrodynamic diameter of ~10.6 nm and 11.6 nm for AGuIX@PS@scramble and AGuIX@PS@KDKPPR, respectively, which is widely suitable for renal excretion. Besides, magnetic properties of all conjugated-nanoparticles were consistent with their use as a positive contrast agent by MRI analysis with, for instance concerning AGuIX@PS@KDKPPR nanoparticle, parameter values of $r1=18.7\ s^{-1}\cdot mM^{-1}$ per Gd^{3+}, $r2/r1=1.6$ at 1.4 T. Accordingly, these relaxometry parameters provided precious information on complexation of Gd^{3+} ions, leading to relatively similar results for our conjugated nanoparticles. DOTA ligands were initially selected due to their relevant affinity for Gd^{3+} (log K=25).[32] Phantom measurements for MRI allowed us to a detection limit of $0.1\ mg.mL^{-1}$. AGuIX nanoparticles displayed longitudinal relaxivity of $6.0\ s^{-1}.mM^{-1}$ twice the value of DOTAREM® (Guerbet, France). The small size of all these nanoparticles grafted or not was obtained by a top-down process.[27]

Regarding to the photophysical properties (Figure 1B), absorption spectra of free PS, corresponding to porphyrin molecules and the different suspensions of nanoparticles with or without peptide, showed comparable profiles. No shift in the maximum absorption at 410 nm was observed. The absorption spectrum characteristic of porphyrin molecule was conserved even after grafting onto nanoparticle with a high absorption band between 350 and 450 nm called the Soret band, and four Q bands (Q_{IV}, Q_{III}, Q_{II} and Q_I). Concerning fluorescence spectra (Figure 1C), the low decrease of fluorescence emission intensity after coupling indicated that the PS molecules linked onto the silica matrix were slightly affected by the microenvironment. Using the fluorescence intensity of the PS related to its concentration, we estimated that each AGuIX nanoparticle contained approximately one or two porphyrin molecules. Calibration curves also indicated that one PS@KDKPPR compound was present for 15 Gd^{3+}, corresponding to one to two nanoparticles (data not shown). Because of the poor solubility of PS such as porphyrin molecules in a hydrophilic medium, we used a solution of D_2O for fluorescence (Φ_F) and singlet oxygen (Φ_Δ) quantum yields measurements for all compounds. No significant change has been measured for free or conjugated-nanoparticles Φ_F and Φ_Δ (Table 1). The percentages of Φ_Δ achieved on average 58% for AGuIX@PS versus 28% for AGuIX@PS@KDKPPR. Concretely, after excitation at 418 nm, AGuIX@PS nanoparticles produced more singlet oxygen than the other peptide-conjugated nanoparticles. In closing, as presented in Table 1, nanoparticles conjugated with KDKPPR or scramble peptide, present relevant photophysical characteristics to induce a photodynamic effect.

Zeta potential values are given on Figure 1D. At pH greater than 6.0, functionalized AGuIX nanoparticles exhibit a negative charge justified by the fact that the peptide grafting leads to the loss of the amino-protecting group which could be protonated at low pH and the addition of carboxylate function of aspartic acid on the peptide. In addition, at high pH lower potential values were obtained as a positive protonable function was removed and a negative carboxylate was added. Moreover, porphyrin molecule is very hydrophobic and could therefore greatly modify the solvation sphere around AGuIX nanoparticle. In principle, cationic nanoparticles have higher affinity for macrophages than neutral and anionic nanomaterials.[33] Attachment of surface protein, such as opsonins may result in opsonization and subsequent phagocytosis. The negative zeta potential of the AGuIX@PS@KDKPPR nanoparticle characterizes its surface charge, which is essential for preventing opsonization in vivo and contributes to successfully achieve an effective targeting.

SPR Experiments

Using SPR, we evaluated the affinities of KDKPPR and scramble free peptides, and also peptides-conjugated AGuIX nanoparticles to recombinant rat and human NRP-1 proteins; optical biosensors based on SPR

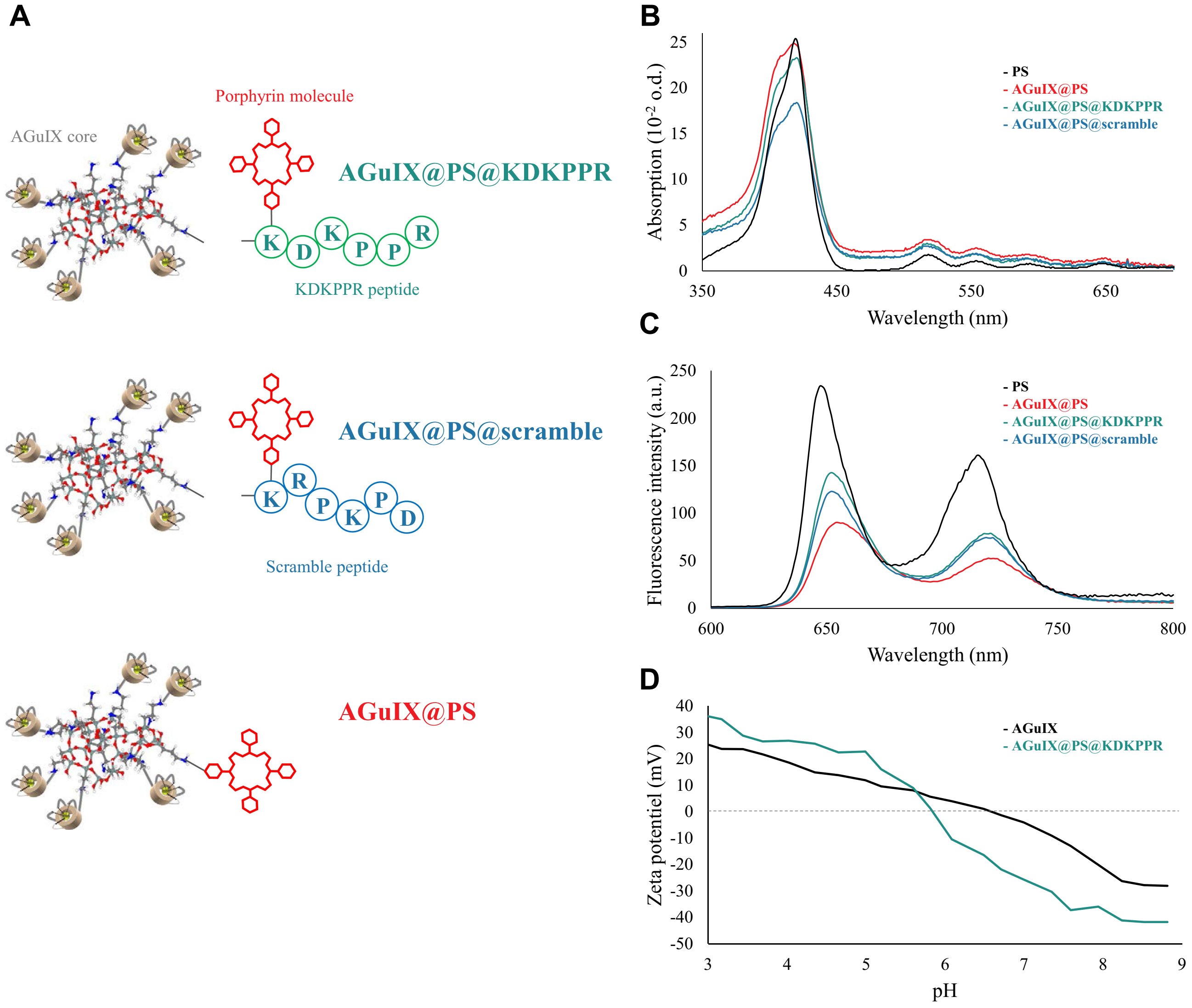

Figure 1 Photophysical properties and physicochemical characterization of the different compounds. (**A**) Schematic representation of the different functionalized nanoparticles AGuIX@PS@KDKPPR (in green), AGuIX@PS@scramble (in blue), AGuIX@PS (in red) and porphyrin (in black). The nanoplatform is made up of the original AGuIX with polysiloxane core containing chelated Gd grafted to the inorganic matrix as contrast agent for MRI, a porphyrin as PS and KDKPPR peptide for NRP-1 receptor targeting versus a scrambled peptide as negative control. (**B**) Absorption spectra and (**C**) fluorescence emission spectra for the three nanoparticles and the free PS (in black) (λ_{exc} = 418 nm). (**D**) Evolution of zeta potential as a function of pH for AGuIX and AGuIX@PS@KDKPPR nanoparticles.

Abbreviations: Gd, gadolinium; MRI, magnetic resonance imaging; NRP-1; neuropilin-1; PS, photosensitizer.

detection helped to obtain information about interaction and binding affinity between analytes such as peptides and small nanoparticles and target protein covalently attached to the surface of a sensor chip. Fits of the response versus analyte concentrations allowed to determine K_{Ds} to a 1:1 binding model. As shown in Figure 2, analysis of the SPR data allowed us to determine affinities. The best affinity was determined for the human NRP-1 – KDKPPR peptide interaction (K_D 0.5 µM, Table 2). The grafting of KDKPPR onto nanoparticle induced a decrease of affinities from 0.5 to 4.7 µM and from 8.7 to 25.2 µM for human and rat NRP-1 proteins, respectively. Finally, scrambled control peptide did not bind to NRP-1 recombinant proteins (see supplementary Figure S1).

In vivo, we already determined VEGF plasma and tumor levels in nude mice xenografted with U87 cells. $VEGF_{121}$ et $VEGF_{165}$ intra-tumor concentrations measured (330 ± 460 pg/mg of proteins) are comparable with the literature. Plasma concentrations (121 and 165 isoforms) were lower than K_D values. Hence, the level of $VEGF_{165}$ in the blood compartment cannot hinder the recognition of ATWLPPR-conjugated nanoparticle by NRP-1.[34] In previous in vivo studies, we highlighted the tropism of

Table 1 Photophysical Properties and Chemical Characteristics of Compounds

	ε (10^3 L.mol^{-1}.cm^{-1})					λ_{exc} (nm)	ϕ_F (%)	ϕ_Δ (%)	Hydrodynamic Diameter (nm)	Relaxometry (60 mHz 37°C) r_1 (s^{-1}.mM^{-1})	Zeta Potential (mV)
	Soret band	Q_{IV}	Q_{III}	Q_{II}	Q_I						
AGuIX	–	–	–	–	–	–	–	–	4.9 ± 1.4	r_1 = 18.3 r_2/r_1 = 1.4	−9.1
PS	224.0	15.1	7.8	5.3	4.5	418	15	24	–	–	–
AGuIX@PS	124.5	17.0	12.5	9.0	7.0	418	7	58	11.2 ± 3.9	r_1 = 16.1 r_2/r_1 = 1.6	–
AGuIX@PS @KDKPPR	116.5	15.0	9.0	6.5	5.0	418	10	28	11.6 ± 6.3	r_1 = 18.7 r_2/r_1 = 1.6	−30.3
AGuIX@PS @scramble	92.0	13.5	9.5	7.0	5.0	418	9	35	10.6 ± 2.3	r_1 = 15.4 r_2/r_1 = 1.6	–

Abbreviations: PS, photosensitizer; ε, molar extinction coefficient; λ_{exc}, excitation wavelength; ϕ_F fluorescence quantum yields; ϕ_Δ, singlet oxygen quantum yields; - not assessable.

ultrasmall nanoparticles targeting NRP-1 via ATWLPPR peptide.[26] This heptapeptide was also specific for NRP-1,[35] allowing efficient tumor tissue uptake despite its very low affinity after coupling (19 µM for the heptapeptide alone versus 171 µM after coupling).[36] In order to improve the selectivity, this new peptide moiety KDKPPR has been designed and optimized by our group from a screening methodology.[29] This peptide sequence was based on the sequence homology of the domain encoded by exon 8a of VEGF$_{165}$ and lysine amino acid was added in order to allow its grafting without affecting the affinity. A docking analysis combined with biological evaluations, hydrogen bond and π-π interactions have been highlighted between NRP-1 protein (PDB ID: 2ORZ) and DKPPR especially with Y297 D320 S346 E348 T349 and Y353 peptides.

Vascular Selectivity Using the Cranial Chamber Model in Mice

Using spheroids of U87-GFP implanted in the healthy brain parenchyma of nude mice, we highlighted the in vivo selectivity for KDKPPR-conjugated nanoparticles towards the tumor endothelium and their systemic comportment (Figure 3A). This original model allowed us the visualization of the nanoparticles by red fluorescence corresponding to the PS and, to estimate the mean residual time into the tumor vasculature. In both cases, one-hour post-injection, peptide-conjugated nanoparticles were mostly colocalized into the blood compartment whereas in later times, only AGuIX@PS@KDKPPR remained in the tumor vasculature probably into endothelial cells lining the vasculature (Figure 3B). As the endothelial angiogenic cells are the intended cell targets, these tumor data supported an irradiation time in the first hour's post-injection of AGuIX@PS@KDKPPR in order to take advantage of maximal concentrations of the PS in the endothelium.

Tumor Tissue Accumulation in Xenografted Nude Rats

Tissue contrasts in MRI are defined by two temporal characteristics which are T1-weighted and T2-weighted images, often referred to as T1 and T2 images. The timing of radiofrequency pulse sequences used to make T1 images results in images which highlight fat tissue within the body. T1 image reflects the time needed by protons to recover their initial maximum magnetization M0. Tissues with long T1 recovering faster than others, they appear brighter on the images. On the contrary, T2 image is the time needed to decrease the signal from the maximum transverse magnetization to the idle state. Tissues with short T2 decreasing faster than others, they appear darker on the images. Nevertheless, external factors such as magnetic field inhomogeneity, decrease the T2 relaxation time and the recorded signal is thus called T2* (* standing for "apparent" T2). The introduction of paramagnetic agents, such as Gd contrast agents, decrease T1 and T2, resulting in structures brighter on T1 images while they appear darker on T2 images. Thanks to the Gd contained in AGuIX-design nanoparticle, T1-weighted morphological sequence by MRI allowed us to follow the signal intensity enhancement (visible in white, Figure 4A) after their i.v. injection. The increase in signal intensity, visible

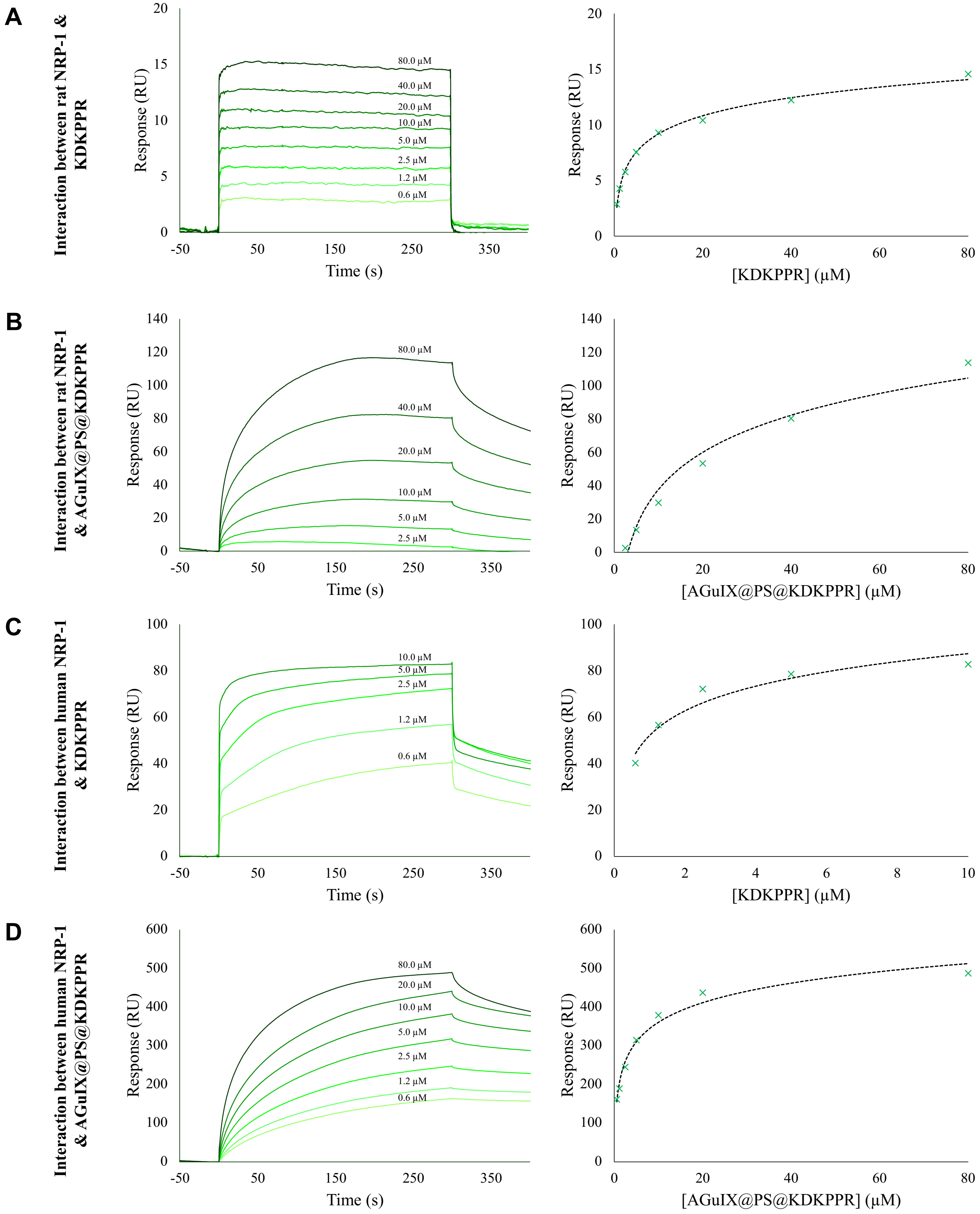

Figure 2 SPR experiments. Sensorgrams (left) and titration (right) curves corresponding to the interaction between (**A**) rat NRP-1 and KDKPPR peptide, (**B**) rat NRP-1 and AGuIX@PS@KDKPPR nanoparticles, (**C**) human NRP-1 and KDKPPR peptide, and (**D**) human NRP-1 and AGuIX@PS@KDKPPR nanoparticles. Briefly, IgG1 (4020 RU), recombinant rat (9556 RU) and human (10124 RU) NRP-1 proteins were immobilized on a CM5 sensor chip. The KDKPPR peptides or the AGuIX@PS@KDKPPR nanoparticles were used as analytes and injected at concentrations ranging from 0.625 to 80 µM at a flow rate of 30 µL.min^{-1} at temperature of 25°C. Sensorgrams (responses as a function of time) were used to draw titration curves by plotting responses recorded 5 s before the end of injection as a function of analyte concentrations.
Abbreviations: IgG1, immunoglobulin G1; NRP-1; neuropilin-1; SRP, surface plasmon resonance.

Table 2 Dissociation Constant (K_D) Values of the Peptide KDKPPR Alone or Grafted Onto AGuIX Nanoparticles for Recombinant Rat or Human NRP-1 Proteins

Compounds	K_D (μM)	
	Rat NRP-1	Human NRP-1
KDKPPR	8.7	0.5
AGuIX@PS@KDKPPR	25.2	4.7

Note: NRP-1, neuropilin-1.

immediately after their injection, lasted up to 24h regardless of the nanoparticle. The improvement of the tumor signal intensity seemed more substantial for the two grafted nanoparticles (Figure 4B). T2*-weighted perfusion MRI is based on the so-called "first passage" approach: the modification in the T2*-weighted MRI signal was followed during the first passage of a bolus of nanoparticles. The pixel-by-pixel analysis of the curves was used to obtain parametric maps (time of arrival, time of the peak, mean transit time). Considering the different profiles of signal intensity, the coronal sections allowed us to differentiate original AGuIX nanoparticles from those with peptides (AGuIX@PS@KDKPPR and AGuIX@PS@scramble). For AGuIX nanoparticles, the intensity of the normalized ΔR2* signal decreased by more than 50%, 90 minutes after injection with a MTT of 14.3 ± 1.9 seconds whereas it remained stable/unchanged for the two other peptide-conjugated nanoparticles (Figure 4B). However, no difference was observed between KDKPPR or scramble-conjugated nanoparticles with MTT values of 16.8 ± 0.5 seconds versus 16.6 ± 1.8 seconds, respectively. To assess the kinetics of retention of nanoparticles in the vascular system, this imaging approach by MRI focused on a sequence with high temporal precision to the detriment of spatial resolution. Indeed, measurement of perfusion by T2*-weighted images was mostly restricted by the resolution of the MRI for the voxel size (200 μm) which was too large to exclusively include blood vessels of the tumor vascular network.

In vivo Nanoparticles Biodistribution and Elimination

Whole-body distribution of AGuIX@PS@KDKPPR interest nanoparticle was evaluated in rodents (rats and mice) at the injected concentration of 4 $\mu mol.kg^{-1}$ (porphyrin equivalent) corresponding to 55 $\mu mol.kg^{-1}$ (Gd equivalent) until 96h post-i.v. injection. During all this period, no sign of clinical toxicity was observed. After nanoparticles injection, fluorescence induced by porphyrin molecule was mainly occurred in organs of excretion such as liver, bladder and kidneys with a time-dependent decrease (Figure 5A and B). Nevertheless, fluorescence intensity decreased for all these organs according to time post-injection, excepted for the lymph nodes (Figure 5C and D). The body distribution is governed by the surface properties of the nanoparticles.[37] The physiological impact of a nanomaterial is mainly determined by different factors such as their coatings, zeta potential and size. The physicochemical characteristics of a nanoparticle influence biocompatibility which includes the route of uptake and clearance, cytotoxicity, and reticuloendothelial system (RES) recognition. The reticulohistocytic system, also named RES or mononuclear phagocyte system is a network of cells and tissues that are distributed over the whole body and are especially abundant in the blood, liver, spleen, lungs, lymph nodes, bone marrow, but also in connective tissues and the brain. The cells of the RES take up materials in the blood and in the tissues by phagocytosis and degrade and inactivate these materials with the help of enzymes. This network of cells consequently possesses important functions of the immune defenses against diseases. Lymphatic vessels are also the preferential route of most solid tumors to spread their metastases in the body. These nanoparticles, thanks to their ultrasmall size, could represent suitable carriers for imaging and for transport to the lymphatic vessels. Different nanoparticle delivery systems developed for the detection and treatment of lymphatic metastases have been described.[38] Accordingly, KDKPPR-conjugated AGuIX nanoparticle could also be a promising approach for the detection and treatment of lymphatic metastases.

Owing to the presence of Gd chelates in AGuIX nanoparticles, the excretion mode was also carried out using MRI analysis post-injection of KDKPPR-conjugated nanoparticles (Figure 6). We followed their in vivo biodistribution before, 1, 4 and 24 hours after i.v. injection. A positive contrast enhancement of the MRI signal intensity was only observed for the kidneys and the bladder (Figure 6A). The concentration of Gd has also shown high levels in the kidneys and in the liver (Figure 6B). At 24h post-injection, organs with the highest Gd concentrations were indeed kidneys and liver with 13.9% and 7.3% of the ID, respectively. As expected in brains for tumor-free animals, Gd was not detected by ICP-MS results (detection threshold of 0.05% of $ID.g^{-1}$). Our findings are in agreement with preclinical safety studies using original AGuIX nanoparticles. Moreover, their rapid elimination

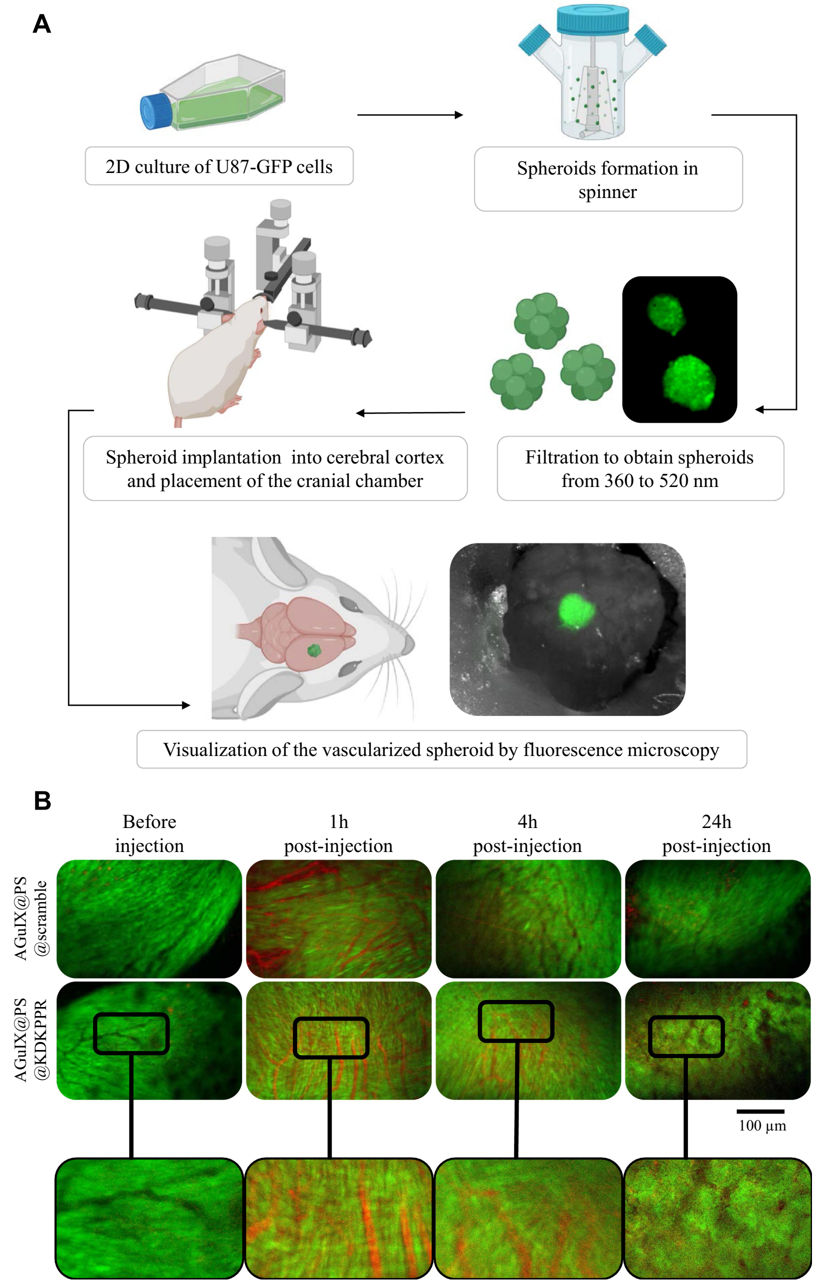

Figure 3 Vascular selectivity using the cranial chamber model with U87-GFP spheroid and fluorescence imaging. (**A**) Experimental protocol illustrating spheroids formation (U87-GFP cells grown in non-adherent flasks were transferred to a spinner placed on a magnetic stirrer for 4 days to form spheroid), their filtration and implantation onto the cerebral cortex of nude mice. A glass window was placed on the skull allowing visualization of the tumor tissue and its vasculature at about 10 days after xenotransplant. Mice were divided into two batches: AGuIX@PS@KDKPPR or AGuIX@PS@scramble group. Visualization of different nanoparticles into the vasculature was performed on anesthetized mice. Blood vessels are observed in black and PS fluorescence in red. (**B**) The vascular network was imaged before, 1, 6 and 24h after i.v. injection of nanoparticles ($4\ \mu mol.kg^{-1}$, porphyrin equivalent). The excitation filter was at 560 ± 25 nm and at 475 ± 20 nm for PS and GFP-U87 fluorescent images acquisition, respectively. The emission filter was composed with a block of four emission filters at 440, 521, 607 and 700 nm. Photos taken with the same magnification; scale bar represents 100 µm.

Abbreviations: GFP, green fluorescent protein; i.v., intravenous; PS; photosensitizer.

from blood circulation by kidneys has been highlighted suitable to limited potential toxic effects.[9,39] Indeed, recently, the European Medicines Agency recently recommended the restriction of the use of Gd-based contrast agents due to their cerebral deposition and their possible serious side effects such as nephrogenic systemic fibrosis.[40] Uncomplexed, Gd^{3+} cations can lead to direct damage of the tissue due to their insolubility and their ability to complete with calcium ions and blockage of voltage dependent calcium channels (inhibition of vital

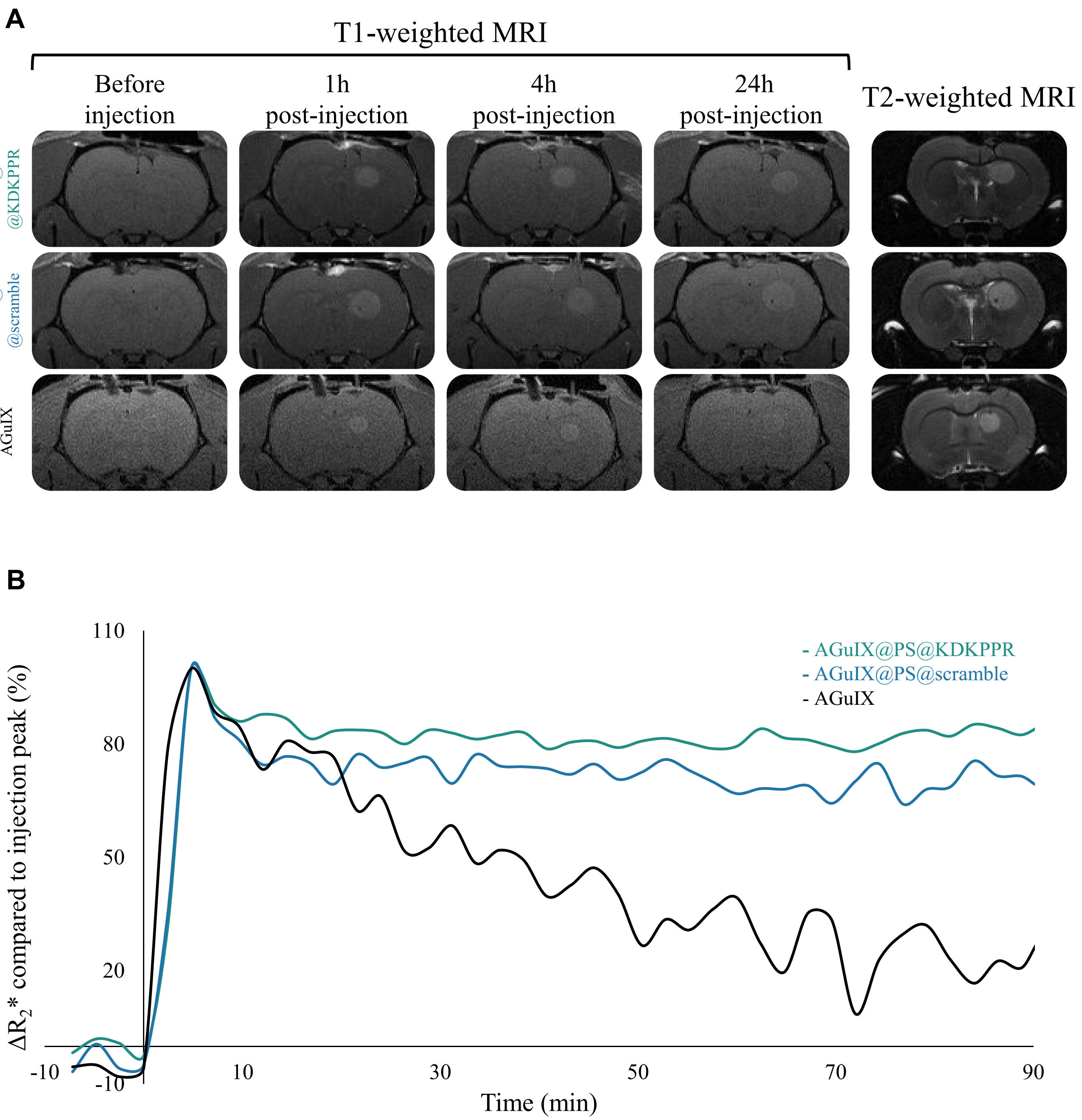

Figure 4 Tumor tissue selectivity of nanoparticles using MRI analysis in xenografted nude rats. (**A**) Axial T2- and T1- weighted MRI before, 1, 4 and 24h after i.v. injection of AGuIX@PS@KDKPPR, AGuIX@PS@scramble or AGuIX nanoparticles (80 μmol.kg^{-1}, Gd equivalent). Proton density weighted MRI (TR/TE: 5000/33 ms, NEX: 2, FOV: 4×4 cm, matrix: 256×256, slice thickness: 1 mm). (**B**) Monitoring of the $\Delta R2^*$ relaxivity after injection of AGuIX@PS@KDKPPR (in green), AGuIX@PS@scramble (in blue) and original AGuIX nanoparticles (in black). The continuous T2*-weighted sequence over 90 minutes produced 45 images in coronal section. Each MRI images made it possible to establish the mapping of the $\Delta R2^*$ relaxivity over time which was then normalized with the signal in the cerebellum (data points show the mean, n = 3).
Abbreviations: FOV, field of view; Gd, gadolinium; MRI, magnetic resonance imaging; NEX, number of excitations; TE, echo time; TR, repetition time; $\Delta R2^*$, measured relaxivity change.

physiological processes such as breathing, heartbeat, muscle contraction or transmission of nerve impulses). The use of macrocyclic compounds such as Gd-DOTA, which tend to lower dechelation compared to linear compounds, limit the release of free Gd^{3+} due to their strong complexation ability (logβ110 = 25.58) and their favorable kinetic of chelation.[9] Despite persistence of Gd in the kidneys until one week (data not shown) no toxicity was evidenced (no microscopic changes as vacuolation) as mentioned after two administrations of nanoparticles at a high dose of 450 mg.kg-1 in the cynomolgus monkeys.[9] One of the main purposes of this study was to establish how the

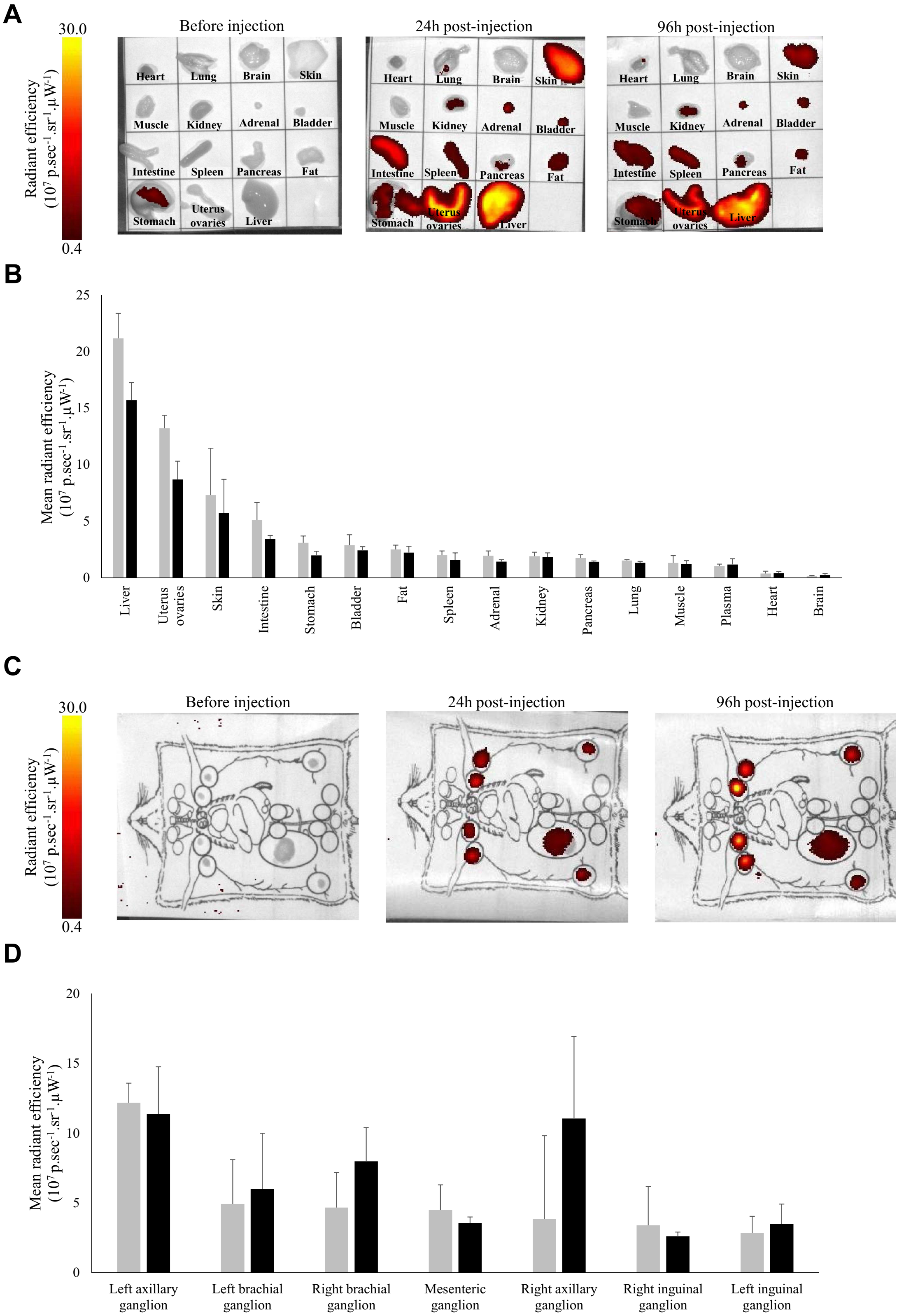

Figure 5 In vivo nanoparticles whole body biodistribution and elimination by fluorescence imaging. (**A**) and (**C**) Before and 24 or 96h after i.v. injection of AGuIX@PS@KDKPPR (4 µmol.kg^{-1}, porphyrin equivalent) nanoparticles in nude mouse organs, lymph nodes and plasma were collected and weighed. All organs were visualized using the 2D optical tomography IVIS® Kinetic (λ_{exc}430 nm/λ_{em}720 nm). (**B**) and (**D**) Quantification of fluorescence emission intensities whole body intensity 24h (dark gray) and 96h (black) after injection are shown on histograms. Bars represent the average of three different animals for each time point (data points show the mean ± SD, n = 3).

Abbreviations: 2D, 2 dimensional; i.v., intravenous; SD, standard deviation.

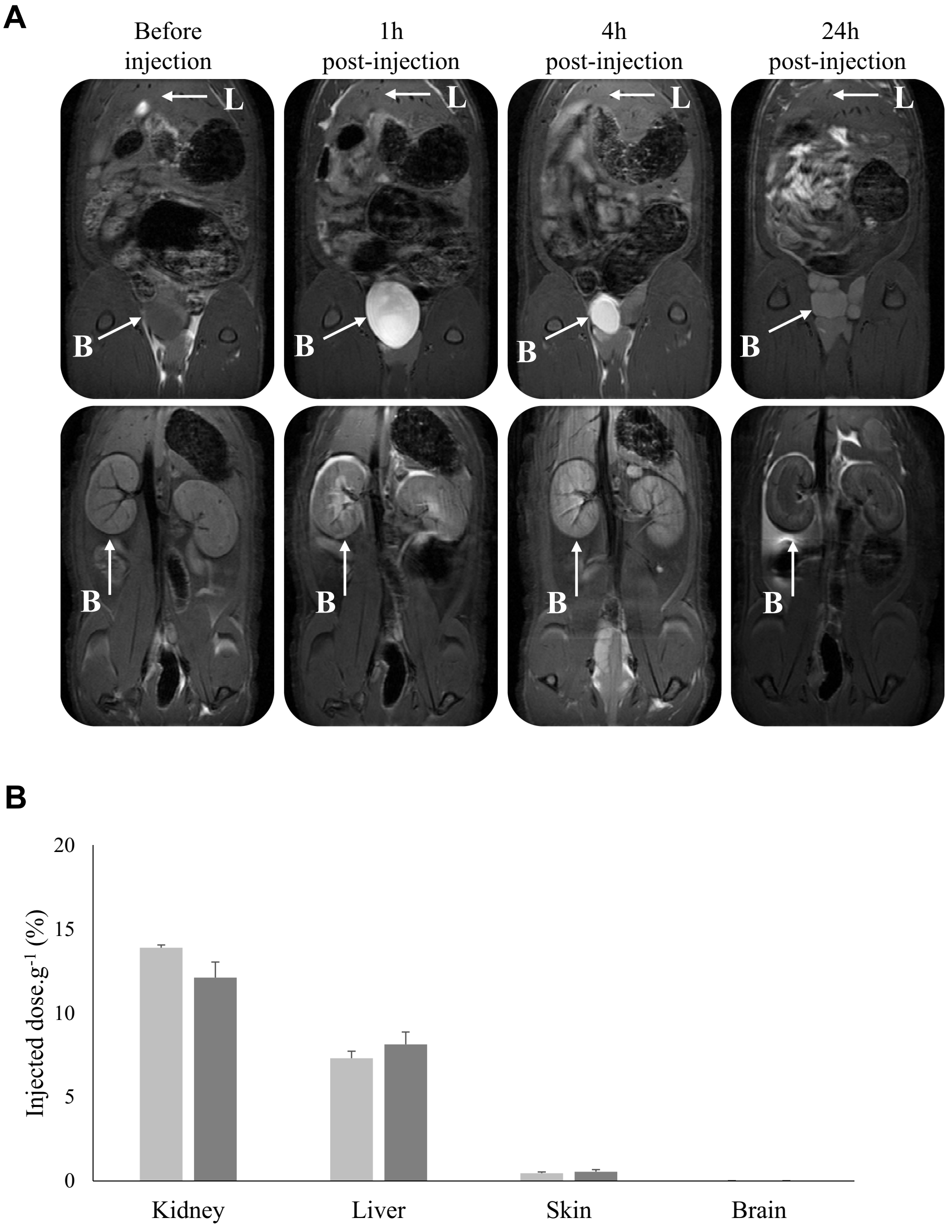

Figure 6 (**A**) Abdominal biodistribution visualized with dynamic T1-weighted image acquisition 1, 4 or 24 h after i.v. injection (80 μmol.kg-1, Gd equivalent for a body weight of 250 g) in the caudal vein of KDKPPR-conjugated nanoparticles. The parameters of the sequence were: TR/TE = 400/9 ms, 80 mm square FOV, matrix 256 × 256. 16 slices of 1.5 mm without interslice gap allowed detecting nanoparticles in kidneys and bladder. A positive MRI signal appeared in the renal cortex of kidneys and the bladder. (**B**) Gadolinium concentrations were evaluated in each organ by ICP-MS. The organs were collected 24h (light gray) and 72h (dark gray) after injection. Bars represent the average percent of the injected dose per gram of three different animals for each time point (data points show the mean ± SD, n = 3).

Abbreviations: FOV, field of view; Gd, gadolinium; ICP-MS, inductively coupled plasma mass spectroscopy; i.v., intravenous; MRI, magnetic resonance imaging; SD, standard deviation; TE, echo time; TR, repetition time.

grafting of a rather hydrophobic element such as porphyrin (partition coefficient (Log P) of 2.6)[30] and a peptide onto the AGuIX silica skeleton could modify/impact their pharmacokinetic parameters. We validated that the elimination of KDKPPR-conjugated nanoparticle by the renal route was not affected by the grafting. The nanoparticles, which are polysiloxane skeleton part surrounded by Gd chelates, pass directly from the kidney to the bladder while the entire AGuIX are retained by renal cortical cells.[41,42] Although in a lower proportion compared to the tumor vascular network, the basal protein expression of NRP-1 in healthy tissues could have an impact on functionalized nanoparticles distribution. In humans, NRP-1 protein expression has been indeed detected in uterus, liver, and gastrointestinal tract.[43] Moreover, NRP-1 has been shown to be strongly expressed in small diameter blood vessels of myometrial and endometrial compartments of the uterus in rat.[44] Moreover, it is also possible that at high dilution in biological fluids, the biodegradation of the silica skeleton of AGuIX nanoparticles may explain the fluorescence signal of porphyrin measured in different organs such as the liver and skin.

In vivo Efficiency Post-iPDT

After i.v. injection of KDKPPR-conjugated AGuIX nanoparticles, tumor tissue was visualized by T1-weighted imaging and then illuminated by interstitial stereotactic PDT. Compared to control, the percentage of tumors not having reached two times their initial volume was statistically significantly increased with interstitial PDT using AGuIX@PS or AGuIX@PS@KDKPPR (Figure 7A). Moreover, the vascular targeting strategy with our nanoparticles led to a statistically significantly more prolonged time in tumor growth delay ($p<0.0001$) of 13 days with KDKPPR peptide instead of 7 days without functionalization by the affin peptide. Before and after treatment with AGuIX@PS@KDKPPR nanoparticle, ^{18}F-FDG-PET analysis was realized for each treated animal (Figure 7B). ^{18}F-FDG uptake reflects tumor metabolism. Healthy brain tissue was thus chosen as reference to calculate the SUV ratio. The calculated values of the tumor metabolism after treatment decreased from 1.5 (just before PDT) to 0.9 and 0.8 at 24h and 72h post-treatment, respectively. Moreover, we also demonstrated that an inflammatory reaction post-VTP may be secondary to an ischemic-related cell death.[25]

VTP aims to activate the PS in order to react with molecular oxygen present in tumor-associated endothelial cells lining the tumor-associated blood vessels, inducing microvascular dysfunction by occlusion and ischemia processes. Consequently, the oxygen and nutrients transported through the tumor vessels decreased rapidly and led to a consecutive tumor necrosis.[45] This strategy can also be performed by reducing the drug light interval, when the PS is not yet incorporated and present in the vessels or by targeting specific receptors over-expressed by endothelial cells.[46] In this study, we demonstrated relevant results of an in vivo treatment efficiency with a prolonged delay in tumor growth accompanied by a decrease of tumor metabolism within a few days after VTP. However, these temporary effects motivate a repetitive treatment in order to lead to a brain tumor cure.

Some work has demonstrated that PDT would not only destroy primary tumor but at the same time strengthen recognition of the remaining tumor cells by the immune system.[47] In addition, the vascular niche was shown to interfere with irradiation therapies by shielding the CSCs.[48] It was demonstrated that the CSCs can secrete growth factors such as VEGF, promoting angiogenesis and thereby enhancing tumor growth. NRP-1 has received significant attention as a potential therapeutic target in GBM. Increased NRP-1 expression in GBM biopsies correlates with increased malignancy, whereas reducing its expression suppresses migration, proliferation and survival in vitro, and CSCs viability and tumor growth in vivo.[17,49] NRP-1 has also been shown to function as a co-receptor for VEGF-R on GAM where it plays a key role in the accumulation of immunosuppressive and pro-angiogenic macrophages. NRP-1 is also mainly implicated in GAM immune polarization, exhibiting a decrease in anti-tumorigenic GAMs infiltrate. GAM is now recognized as an integral part of GBM progression, and as such, pre-clinical therapies that modulate these cell populations aim to harness their properties to slow or reverse tumor growth.[50,51] NRP-1 signaling in monocytic cells, such as GAM, is not well characterized but it has previously shown that GAM-specific ablation of NRP-1, or global pharmacological inhibition of this receptor, slows tumor progression in a mouse model of GBM, in a similar fashion, by inhibiting angiogenesis and reducing immunosuppressive signaling. Further, it has been reported that either population of microglia or peripheral macrophages lacking NRP-1, were enough to inhibit GBM progression.[49,52] How KDKPPR-functionalized AGuIX nanoparticles could affect macrophage polarization could also be an interesting approach for understanding the regulatory effects on immune cells in vivo.

Conclusion and Perspectives

In this work, we proposed ultrasmall theranostic AGuIX nanoparticle for VTP of GBM. Using original multimodal and multiscale approaches, we first validated the molecular affinity of KDKPPR-conjugated AGuIX nanoparticle to NRP-1 protein and secondarily, to the tumor vascular network using an original cranial chamber model in mice. Compared to scramble conjugated AGuIX nanoparticles as control, we confirmed that their grafting with KDKPPR promoted a localization into the tumor vessel wall, highlighting their potential for a VTP guided by MRI.

In vivo results also revealed promising interests with an extended time of tumor growth retardation and a decrease in tumor metabolism after treatment. PDT is also well known for inducing indirect effects from various non-malignant components of the tumor

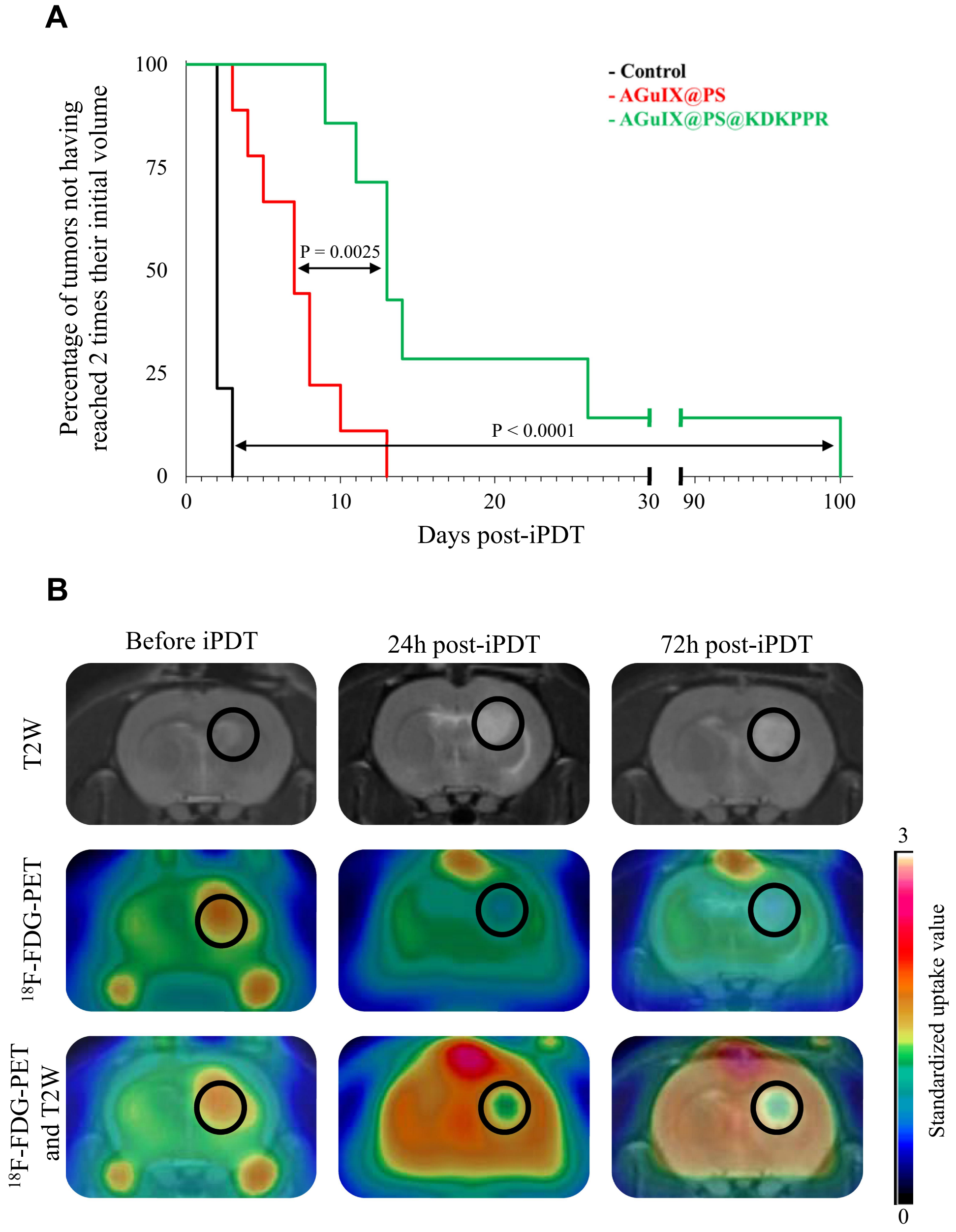

Figure 7 In vivo efficiency post-iPDT. (**A**) Kaplan–Meier curves of control rats or rats treated by PDT using AGuIX@PS nanoparticles (in red) or AGuIX@PS@KDKPPR (in green), considering the percentage of tumors not having reached 2 times their initial volume at the end point. At least seven animals were used for each experimental group. Statistical analysis was performed using the Log rank test and highlighted a statistically significant difference between AGuIX@PS@KDKPPR group and control group ($p < 0.0001$) and between AGuIX@PS ($p=0.0025$). (**B**) MRI images and ^{18}F-FDG PET images in axial view before, 24 and 72h after PDT with AGuIX@PS@KDKPPR. The tumor tissue is indicated in the black circle.

Abbreviations: ^{18}F-FDG, Fluorine-18 fluorodeoxyglucose; iPDT, interstitial photodynamic therapy; MRI, magnetic resonance imaging; PDT, photodynamic therapy; PET, positron emission tomography.

microenvironment such as the inflammatory process, leading to cytotoxic and vasogenic edema, ischemia and antiproliferative activity via the expression of several inflammatory mediators. In complement to PET-CT analyses, the apparent diffusion coefficient (ADC) mapping by MRI could provide us precious locoregional information to localize vasogenic edema due to tissue necrosis.[25]

NRP-1 also functions as a receptor on GAM where it plays a key role in the accumulation of immunosuppressive and pro-angiogenic macrophages. Thus, how PDT targeting NRP-1 affects the accumulation of macrophages would be crucial to understand treatment effects on immune cells. Finally, the NRP-1 targeting strategy with AGuIX nanoparticle could also be extended to other approaches, notably diagnostic, thus perfecting the detection of tumors and the evaluation of the response to treatments.

Abbreviations

2D, 2 dimensional; 3D, 3 dimensional; ADC, apparent diffusion coefficient; CO$_2$, carbon dioxide; CSC, cancer stem cells; D$_2$O, deuterium oxide; DLI, drug-light interval; DLS, dynamic light scattering; DMSO, dimethylsulfoxide; DOTA, 1,4,7,10-tetraazacyclododecane-1,4,7,10-tetraacetic acid; EDC, 1-ethyl-3-[3-dimethylaminopropyl] carbodiimide; EPR enhanced permeability and retention; FDG, fluorine-18 fluorodeoxyglucose; FOV, field of view; GAM, glioma-associated macrophages; GBM, glioblastoma; Gd, gadolinium; GFP, green fluorescent protein; HNO$_3$, nitric acid; i.v., intravenous; ICP-MS, inductively coupled plasma mass spectroscopy; ID, injected dose; IgG, immunoglobulin G; iPDT, interstitial photodynamic therapy; KD, dissociation constant; Log P, partition coefficient; MRI, magnetic resonance imaging; MTT, mean transit time; NaCl, sodium chloride; NaOH, sodium hydroxide; NEX, number of excitations; NRP-1, neuropilin-1; PBS, phosphate-buffered saline; PDT, photodynamic therapy; PET-CT, positron emission tomography with computed tomography; polyHEMA, poly hydroxyethylmethacrylate; PS, photosensitizer; R.L.U., relative light units; RES, reticuloendothelial system; RNA, ribonucleic acid; ROI, region of interest; SD, standard deviation; SEM, standard error of the mean; SPR, surface plasmon resonance; SUV, standardized uptake values; TE, echo time; TLC, thin-layer chromatography; TR, repetition time; VEGF, vascular endothelium growth factor; VOI, volume of interests; VTP, anti-vascular effect of photodynamic therapy; WBRT, whole brain radiation therapy; $\Delta R2^*$Measured relaxivity change; Φ_F, fluorescence quantum yield; Φ_Δ, singlet oxygen quantum yield.

Acknowledgments

This article was supported by the research funds of the French Ligue Nationale Contre le Cancer, Région Lorraine and EURONANOMED II “PhotoBrain” and “NanoBIT” projects no. ANR-14-ENM2-0001-01 and 447/15/GM, respectively.

Disclosure

F Lux, and O Tillement have one patent to disclose: WO2011135101. This patent protects some of the nanoparticles described in this publication: AGuIX. François Lux reports grants and personal fees from NH TherAguix, outside the submitted work. Olivier Tillement reports grants and personal fees from NH TherAguix, outside the submitted work The authors have no other relevant affiliations or financial involvement with any organization or entity with a financial interest in or financial conflict with the subject matter or materials discussed in the manuscript apart from those disclosed and report no other potential conflicts of interest for this work.

References

1. Weller M, Cloughesy T, Perry JR, Wick W. Standards of care for treatment of recurrent glioblastoma—are we there yet? *Neuro Oncol*. 2013;15(1):4–27. doi:10.1093/neuonc/nos273
2. Stupp R, Weller M, Belanger K, et al. Radiotherapy plus Concomitant and Adjuvant Temozolomide for Glioblastoma. *N Engl J Med*. 2005;10.
3. Dhermain F. Radiotherapy of high-grade gliomas: current standards and new concepts, innovations in imaging and radiotherapy, and new therapeutic approaches. *Chinese Journal of Cancer*. 2014;33(1):16–24. doi:10.5732/cjc.013.10217
4. Wen PY. Malignant Gliomas in Adults. *N Engl J Med*. 2008;16.
5. de Robles P, Fiest KM, Frolkis AD, et al. The worldwide incidence and prevalence of primary brain tumors: a systematic review and meta-analysis. *Neuro Oncol*. 2015;17(6):776–783. doi:10.1093/neuonc/nou283
6. Pinel S, Thomas N, Boura C, Barberi-Heyob M. Approaches to physical stimulation of metallic nanoparticles for glioblastoma treatment. *Adv Drug Deliv Rev*. 2019;138:344–357. doi:10.1016/j.addr.2018.10.013
7. Verry C, Sancey L, Dufort S, et al. Treatment of multiple brain metastases using gadolinium nanoparticles and radiotherapy: NANO-RAD, a Phase I study protocol. *BMJ Open*. 2019;9(2):e023591. doi:10.1136/bmjopen-2018-023591
8. Radiotherapy of Multiple Brain Metastases Using AGuIX$^{®}$ (NANORAD2). https://clinicaltrials.gov/ct2/show/NCT03818386. Accessed October 20, 2020.
9. Kotb S, Piraquive J, Lamberton F, et al. Safety Evaluation and Imaging Properties of Gadolinium-Based Nanoparticles in nonhuman primates. *Sci Rep*. 2016:6. doi:10.1038/srep35053
10. Evaluating AGuIX$^{®}$ Nanoparticles in Combination With Stereotactic Radiation for Brain Metastases (NANOSTEREO) https://clinicaltrials.gov/ct2/show/NCT04094077?term=NCT04094077&draw=2&rank=1. Accessed October 20, 2020.
11. Lux F, Tran VL, Thomas E, et al. AGuIX $^{®}$ from bench to bedside—Transfer of an ultrasmall theranostic gadolinium-based nanoparticle to clinical medicine. *The British Journal of Radiology*. 2018:20180365. doi:10.1259/bjr.20180365
12. Maeda H, Sano Y, Takeshita J, et al. A pharmacokinetic simulation model for chemotherapy of brain tumor with an antitumor protein antibiotic, neocarzinostatin: theoretical considerations behind a two-compartment model for continuous infusion via an internal carotid artery. *Cancer Chemother Pharmacol*. 1981;5(4):243–249. doi:10.1007/BF00434392
13. Sparreboom A. Comparative Preclinical and Clinical Pharmacokinetics of a Cremophor-Free, Nanoparticle Albumin-Bound Paclitaxel (ABI-007) and Paclitaxel Formulated in Cremophor (Taxol). *Clin Cancer Res*. 2005;11(11):4136–4143. doi:10.1158/1078-0432.CCR-04-2291
14. Maeda H. Toward a full understanding of the EPR effect in primary and metastatic tumors as well as issues related to its heterogeneity. *Adv Drug Deliv Rev*. 2015;91:3–6. doi:10.1016/j.addr.2015.01.002
15. Bort G, Lux F, Dufort S, Crémillieux Y, Verry C, Tillement O. EPR-mediated tumor targeting using ultrasmall-hybrid nanoparticles: from animal to human with theranostic AGuIX nanoparticles. *Theranostics*. 2020;10(3):1319–1331. doi:10.7150/thno.37543

16. Sun S, Lei Y, Li Q, et al. Neuropilin-1 is a glial cell line-derived neurotrophic factor receptor in glioblastoma. *Oncotarget*. 2017;8(43):74019–74035. doi:10.18632/oncotarget.18630
17. Hamerlik P, Lathia JD, Rasmussen R, et al. Autocrine VEGF–VEGFR2–Neuropilin-1 signaling promotes glioma stem-like cell viability and tumor growth. *J Exp Med*. 2012;209(3):507–520. doi:10.1084/jem.20111424
18. Caponegro MD, Moffitt RA, Tsirka SE. Expression of neuropilin-1 is linked to glioma associated microglia and macrophages and correlates with unfavorable prognosis in high grade gliomas. *Oncotarget*. 2018;9(86):35655–35665. doi:10.18632/oncotarget.26273
19. Lyons M, Phang I, Eljamel S. The effects of PDT in primary malignant brain tumours could be improved by intraoperative radiotherapy. *Photodiagnosis Photodyn Ther*. 2012;9(1):40–45. doi:10.1016/j.pdpdt.2011.12.001
20. Muragaki Y, Akimoto J, Maruyama T, et al. Phase II clinical study on intraoperative photodynamic therapy with talaporfin sodium and semiconductor laser in patients with malignant brain tumors. *Journal of Neurosurgery*. 2013;119(4):845–852. doi:10.3171/2013.7.JNS13415
21. Shimizu K, Nitta M, Komori T, et al. Intraoperative Photodynamic Diagnosis Using Talaporfin Sodium Simultaneously Applied for Photodynamic Therapy against Malignant Glioma: A Prospective Clinical Study. *Front Neurol*. 2018;9:24. doi:10.3389/fneur.2018.00024
22. Dupont C, Vermandel M. INtraoperative photoDYnamic Therapy for GliOblastomas: study Protocol for a Phase. *Clin Trial*. 2018;6.
23. Bechet D, Mordon SR, Guillemin F, Barberi-Heyob MA. Photodynamic therapy of malignant brain tumours: A complementary approach to conventional therapies. *Cancer Treat Rev*. 2014;40(2):229–241. doi:10.1016/j.ctrv.2012.07.004
24. Calixto GMF, Bernegossi J, de Freitas LM, Fontana CR, Chorilli M. Nanotechnology-Based Drug Delivery Systems for Photodynamic Therapy of Cancer: A Review. *Molecules*. 2016;21(3):3. doi:10.3390/molecules21030342
25. Toussaint M, Pinel S, Auger F, et al. Proton MR Spectroscopy and Diffusion MR Imaging Monitoring to Predict Tumor Response to Interstitial Photodynamic Therapy for Glioblastoma. *Theranostics*. 2017;7(2):436–451. doi:10.7150/thno.17218
26. Bechet D, Auger F, Couleaud P, et al. Multifunctional ultrasmall nanoplatforms for vascular-targeted interstitial photodynamic therapy of brain tumors guided by real-time MRI. *Nanomedicine*. 2015;11(3):657–670. doi:10.1016/j.nano.2014.12.007
27. Thomas E, Colombeau L, Gries M, et al. Ultrasmall AGuIX theranostic nanoparticles for vascular-targeted interstitial photodynamic therapy of glioblastoma. *Int J Nanomedicine*. 2017;12:7075–7088. doi:10.2147/IJN.S141559
28. Youssef Z, Yesmurzayeva N, Larue L, et al. New Targeted Gold Nanorods for the Treatment of Glioblastoma by Photodynamic Therapy. *Journal of Clinical Medicine*. 2019;8(12):2205. doi:10.3390/jcm8122205
29. Kamarulzaman EE, Vanderesse R, Gazzali AM, et al. Molecular modelling, synthesis and biological evaluation of peptide inhibitors as anti-angiogenic agent targeting neuropilin-1 for anticancer application. *J Biomol Struct Dyn*. 2017;35(1):26–45. doi:10.1080/07391102.2015.1131196
30. Kamarulzaman EE, Mohd Gazzali A, Acherar S, et al. New Peptide-Conjugated Chlorin-Type Photosensitizer Targeting Neuropilin-1 for Anti-Vascular Targeted Photodynamic Therapy. *Int J Mol Sci*. 2015;16(10):24059–24080. doi:10.3390/ijms161024059
31. Bouzerar R, Chaarani B, Gondry-Jouet C, Zmudka J, Balédent O. Measurement of choroid plexus perfusion using dynamic susceptibility MR imaging: capillary permeability and age-related changes. *Neuroradiology*. 2013;55(12):1447–1454. doi:10.1007/s00234-013-1290-2
32. Truillet C, Lux F, Tillement O, Dugourd P, Antoine R. Coupling of HPLC with Electrospray Ionization Mass Spectrometry for Studying the Aging of Ultrasmall Multifunctional Gadolinium-Based Silica Nanoparticles. *Anal Chem*. 2013;85(21):10440–10447. doi:10.1021/ac402429p
33. Zhou Y, Dai Z. New Strategies in the Design of Nanomedicines to Oppose Uptake by the Mononuclear Phagocyte System and Enhance Cancer Therapeutic Efficacy. *Chem Asian J*. 2018;13(22):3333–3340. doi:10.1002/asia.201800149
34. Thomas N, Bechet D, Becuwe P, et al. Peptide-conjugated chlorin-type photosensitizer binds neuropilin-1 in vitro and in vivo. *J Photochem Photobiol B*. 2009;96(2):101–108. doi:10.1016/j.jphotobiol.2009.04.008
35. Tirand L, Frochot C, Vanderesse R, et al. A peptide competing with VEGF165 binding on neuropilin-1 mediates targeting of a chlorin-type photosensitizer and potentiates its photodynamic activity in human endothelial cells. *J Controlled Release*. 2006;111(1–-2):153–164. doi:10.1016/j.jconrel.2005.11.017
36. Bechet D, Tirand L, Faivre B, et al. Neuropilin-1 Targeting Photosensitization-Induced Early Stages of Thrombosis via Tissue Factor Release. *Pharm Res*. 2010;27(3):468–479. doi:10.1007/s11095-009-0035-8
37. Bantz C, Koshkina O, Lang T, et al. The surface properties of nanoparticles determine the agglomeration state and the size of the particles under physiological conditions. *Beilstein J Nanotechnol*. 2014;5:1774–1786. doi:10.3762/bjnano.5.188
38. Millart E, Lesieur S, Faivre V. Superparamagnetic lipid-based hybrid nanosystems for drug delivery. *Expert Opin Drug Deliv*. 2018;15(5):523–540. doi:10.1080/17425247.2018.1453804
39. Sancey L, Kotb S, Truillet C, et al. Long-Term *in Vivo* Clearance of Gadolinium-Based AGuIX Nanoparticles and Their Biocompatibility after Systemic Injection. *ACS Nano*. 2015;9(3):2477–2488. doi:10.1021/acsnano.5b00552
40. Pasquini L, Napolitano A, Visconti E, et al. Gadolinium-Based Contrast Agent-Related Toxicities. *CNS Drugs*. 2018;32(3):229–240. doi:10.1007/s40263-018-0500-1
41. Le Duc G, Roux S, Paruta-Tuarez A, et al. Advantages of gadolinium based ultrasmall nanoparticles vs molecular gadolinium chelates for radiotherapy guided by MRI for glioma treatment. *Cancer Nanotechnol*. 2014;5(1):1. doi:10.1186/s12645-014-0004-8
42. Mignot A, Truillet C, Lux F, et al. A Top-Down Synthesis Route to Ultrasmall Multifunctional Gd-Based Silica Nanoparticles for Theranostic Applications. *Chem Eur J*. 2013;19(19):6122–6136. doi:10.1002/chem.201203003
43. Tissue expression of NRP1 - Summary - The Human Protein Atlas. Accessed July 1, 2020. https://www.proteinatlas.org/ENSG00000099250-NRP1/tissue.
44. Richeri A, Vierci G, Martínez GF, Latorre MP, Chalar C, Brauer MM. Neuropilin-1 receptor in the rapid and selective estrogen-induced neurovascular remodeling of rat uterus. *Cell Tissue Res*. 2020. doi:10.1007/s00441-020-03196-8
45. Guan M, Zhou Y, Liu S, et al. Photo-triggered gadofullerene: enhanced cancer therapy by combining tumor vascular disruption and stimulation of anti-tumor immune responses. *Biomaterials*. 2019;213:119218. doi:10.1016/j.biomaterials.2019.05.029
46. Czabanka M, Parmaksiz G, Bayerl SH, et al. Microvascular biodistribution of L19-SIP in angiogenesis targeting strategies. *Eur J Cancer*. 2011;47(8):1276–1284. doi:10.1016/j.ejca.2011.02.001
47. Acker G, Palumbo A, Neri D, Vajkoczy P, Czabanka M. F8-SIP mediated targeted photodynamic therapy leads to microvascular dysfunction and reduced glioma growth. *J Neurooncol*. 2016;129(1):33–38. doi:10.1007/s11060-016-2143-8

48. Denysenko T, Gennero L, Roos MA, et al. Glioblastoma cancer stem cells: heterogeneity, microenvironment and related therapeutic strategies. *Cell Biochem Funct*. 2010;28(5):343–351. doi:10.1002/cbf.1666
49. Miyauchi JT, Caponegro MD, Chen D, Choi MK, Li M, Tsirka SE. Deletion of Neuropilin 1 from Microglia or Bone Marrow–Derived Macrophages Slows Glioma Progression. *Cancer Res*. 2018;78 (3):685–694. doi:10.1158/0008-5472.CAN-17-1435
50. Pyonteck SM, Akkari L, Schuhmacher AJ, et al. CSF-1R inhibition alters macrophage polarization and blocks glioma progression. *Nat Med*. 2013;19(10):1264–1272. doi:10.1038/nm.3337
51. Jackson CM, Lim M, Drake CG. Immunotherapy for Brain Cancer: recent Progress and Future Promise. *Clin Cancer Res*. 2014;20 (14):3651–3659. doi:10.1158/1078-0432.CCR-13-2057
52. Miyauchi JT, Chen D, Choi M, et al. Ablation of Neuropilin 1 from glioma-associated microglia and macrophages slows tumor progression. *Oncotarget*. 2016;7(9):9. doi:10.18632/oncotarget.6877